

# Golden Ratio entanglement in hexagonally poled nonlinear crystals

Alessandra Gatti<sup>1,2</sup>, Enrico Brambilla<sup>2</sup>, Katia Gallo<sup>3</sup> and Ottavia Jedrkiewicz<sup>1,2</sup>

<sup>1</sup> *Istituto di Fotonica e Nanotecnologie of CNR, Piazza Leonardo Da Vinci 32, Milano, Italy;* <sup>2</sup> *Dipartimento di Scienza e Alta Tecnologia, Università dell'Insubria, Via Valleggio 11, Como, Italy,*

<sup>3</sup> *KTH - Royal Institute of Technology, Roslagstullsbacken 21, 10691 Stockholm, Sweden\**

This work analyses the quantum state of twin photons and twin beams generated by parametric-down conversion in a hexagonally poled photonic crystal, characterized by the simultaneous presence of two nonlinear processes sustained by two vectors of the reciprocal lattice. In those special points of the fluorescence spectrum where the two processes coexist, we show that a tripartite entangled state is realized, equivalent to a single parametric process followed by a beam-splitter. By proper angle tuning a peculiar resonance condition is reached, with a transition to a 4-mode entanglement, dominated by the *Golden Ratio* of the segment  $\phi = (1 + \sqrt{5})/2$ . A maximal coherence between the two nonlinear processes is here established, as the overall process is shown to be equivalent to *two* independent parametric processes followed by a beam-splitter. We offer an interpretation of the occurrence of the golden ratio in this system based on an analogy between the evolution of the light modes and the Fibonacci sequence.

PACS numbers: 42.65.Lm, 42.50.Ar, 42.50.Dv

## INTRODUCTION

Nonlinear photonic crystals, characterized by a two-dimensional periodic modulation of the nonlinear response [1–3], offer a high degree of flexibility for engineering the properties of optical parametric processes, because of the multiplicity of vectors of the nonlinear lattice providing quasi phase matching. When considering the generation of twin photons or twin-beams by parametric down-conversion (PDC), these photonic crystals have shown interesting potentialities as monolithic sources of path entangled photonic states [4–6], and may provide novel compact schemes for continuous-variable quantum technologies [7].

In this work we analyse the quantum state of twin photons and twin beams generated in a hexagonally poled nonlinear photonic crystal (HexNPC) with a quadratic nonlinearity (see [5, 8, 9]). The HexNPC is characterized by the coexistence of two nonlinear processes, sustained by the two fundamental vectors of the reciprocal lattice of the nonlinearity (Fig.1). In the spectral-angular domain of the down-converted light there are special points where phase matching occurs simultaneously for both processes, and where twin photons may originate by either processes. In the high-gain regime the two possibilities add coherently and stimulate each other, giving rise to unusual isolated hot spots in the parametric emission [10–12].

In the quantum domain, we describe a general scenario of tripartite entanglement holding among specific triplets of hot-spots. We show that here the action of the photonic crystal is equivalent to a single nonlinear process generating a pair of entangled twin beams, followed by a 50:50 beam-splitter dividing one of the twin beams into two separated paths. The occurrence of such a situation was already suggested in [5]. In contrast to the analysis performed in [5], which was limited to the two-photon state generated in the spontaneous regime, our study is valid for any photon number, encompassing both the photonic and continuous-variable entanglement, and emphasizes the role of conditional measurements on generating path entanglement.

In a related experimental work [8], we observed that by properly tuning the angle of incidence of the pump laser, it was possible to reach a particular condition, that was referred to as *superresonance*. In such condition, two triplets of hot spots coalesce into four coupled modes, with a sudden enhancement of the brightness of the hot-spots. Indeed, we demonstrated that the rate of growth of parametric light along the crystal increases in these modes by the famous *Golden Ratio* of the segment,  $\phi = \frac{1+\sqrt{5}}{2}$ . In the present work we show that this condition, corresponding to a transverse spatial resonance between the pump and the nonlinear lattice, gives rise to a quadripartite entangled state, and enables the maximal coherence between the two concurrent nonlinear processes characterizing the hexagonal photonic crystal. In this condition we demonstrate that the action of the HexNPC is equivalent to i) *two* independent parametric processes, with different gains  $g_0\phi$  and  $\frac{-g_0}{\phi}$ , generating two pairs of entangled twin beams, ii) followed by an unbalanced beam-splitter that mixes the two processes according to the Golden Ratio.

---

\* Alessandra.Gatti@mi.infn.it

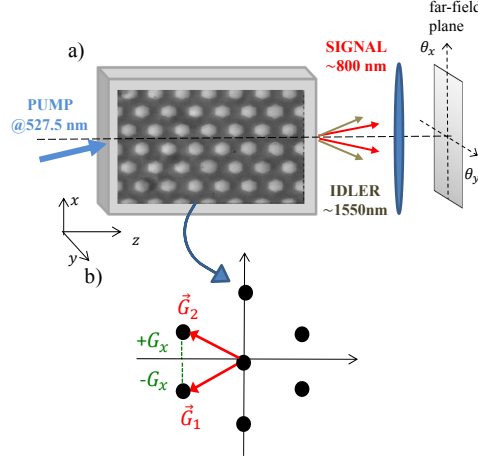


FIG. 1. (a) Scheme of parametric down-conversion in a hexagonally poled nonlinear photonic crystal. The pump beam is allowed to be slightly tilted with respect to the symmetry axis  $z$  of the nonlinear pattern. (b) Vectors of the reciprocal lattice contributing to quasi phase-matching.

An original aspect of our analysis is that it fully takes into account the 3D character of the parametric emission (transverse spatial coordinates plus temporal frequency), by means of extended 3D+1 numerical simulations of the device, complemented by approximated analytical models. This allows us to show that both the 3-mode and 4-mode entanglement can be realized at different frequencies over a broad bandwidth, opening the possibility of a widely tunable implementation of novel quantum states of light.

## I. THE MODEL

We consider the geometry depicted in Fig.1, where a laser pump beam propagates in a  $\chi^{(2)}$  photonic crystal, with a hexagonal pattern of the nonlinear response [5, 8, 9, 12, 13], generating signal and idler waves at lower energies. Light is assumed to propagate mainly along the symmetry axis of the pattern ( $z$ -axis of our frame of reference), but we allow the input pump to be slightly tilted in the pattern plane ( $(x, z)$  plane). Although our analysis may apply to different tuning conditions, we focus on the type 0 process, where all the three waves have the same extraordinary polarization, and on non-degenerate parametric emission, in a configuration similar to the experiment in [14].

The model is formulated in terms of coupled propagation equations for the pump signal and idler field operators, describing three wave-packets centered around frequencies  $\omega_p$ ,  $\omega_s$  and  $\omega_i = \omega_p - \omega_s$ , respectively. The grating of the nonlinearity is described by keeping only the leading order terms in the Fourier expansion of the nonlinear-susceptibility [1, 15]

$$d(x, z) \simeq e^{-iG_z z} [d_{01} e^{-iG_x x} + d_{10} e^{iG_x x}] = 2d_{01} e^{-iG_z z} \cos(G_x x), \quad (1)$$

where only the contribution of the two fundamental vectors of the reciprocal lattice (Fig.1b),  $\vec{G}_1 \equiv \vec{G}_{01} = -G_x \vec{e}_x - G_z \vec{e}_z$  and  $\vec{G}_2 \equiv \vec{G}_{10} = +G_x \vec{e}_x - G_z \vec{e}_z$ , which allow quasi-phase matching (QPM), have been retained. For the hexagonally poled Mg-doped Lithium Tantalate (LiTaO<sub>3</sub>) crystal used in [5, 14],  $d_{10} = d_{01} \simeq 0.29d_{33}$  ( $d_{33} = 17$  pV/m),  $G_z = \frac{2\pi}{\Lambda}$  and  $G_x = \frac{2\pi}{\sqrt{3}\Lambda}$  where  $\Lambda$  is the poling period.

The propagation equations are best written in the Fourier domain spanned by the 3D vector  $\vec{w} = (\vec{q}, \Omega)$ , where  $\vec{q} = q_x \vec{e}_x + q_y \vec{e}_y$  is the wave-vector in the plane transverse to the mean direction of propagation  $z$ , and  $\Omega$  is the frequency shift with respect to the carrier frequencies. The conjugate spatio-temporal domain is in turn described by the vector  $\vec{\xi} = (\vec{r}, t)$ ,  $\vec{r} = x \vec{e}_x + y \vec{e}_y$ , with the convention for the inner product  $\vec{w} \cdot \vec{\xi} := \vec{q} \cdot \vec{r} - \Omega t$ . We consider the three slowly varying envelope operators  $\hat{A}_j(\vec{w}, z) \propto e^{-ik_{jz}(\vec{w})z} \int \frac{d^3 \xi}{(2\pi)^{\frac{3}{2}}} e^{-i\xi \cdot \vec{w}} \hat{E}_j^{(+)}(\xi, z) e^{i\omega_j t}$  for the signal ( $j=s$ ), the idler ( $j=i$ ) and the pump ( $j=p$ ) fields, where  $\hat{E}_j^{(+)}$  are the positive-frequency parts of the respective electric field operators, and  $k_{jz}(\vec{q}, \Omega) = \sqrt{k_j^2(\vec{q}, \Omega) - \Omega^2}$  are the  $z$ -components of the wave-vectors, with the wave number  $k_j(\vec{q}, \Omega) = n_j(\vec{q}, \Omega) \frac{\omega_j + \Omega}{c}$  being determined by the linear dispersion relation of the  $j$ -th wave in the medium. Dimensions

are such that  $\hat{A}_j^\dagger(\vec{w})\hat{A}_j(w)$  are photon numbers per unit frequency and wavevector squared. The field operators  $\hat{A}_j$  are slowly varying along  $z$ , because all the effects of the linear part of the interaction with the medium, contained in  $k_{jz}$ , have been subtracted. Their evolution along the nonlinear photonic crystal is described by the following equations (see [16, 17] for derivations of similar equations):

$$\frac{\partial}{\partial z}\hat{A}_s(\vec{w}_s, z) = \chi \int \frac{d^3\vec{w}_p}{(2\pi)^{\frac{3}{2}}}\hat{A}_p(\vec{w}_p, z) \left[ \hat{A}_i^\dagger(\vec{w}_p - \vec{w}_s - \vec{G}_x, z)e^{-i\mathcal{D}_1(\vec{w}_s, \vec{w}_p)z} + \hat{A}_i^\dagger(\vec{w}_p - \vec{w}_s + \vec{G}_x, z)e^{-i\mathcal{D}_2(\vec{w}_s, \vec{w}_p)z} \right] \quad (2)$$

$$\begin{aligned} \frac{\partial}{\partial z}\hat{A}_i(\vec{w}_i, z) = \chi \int \frac{d^3\vec{w}_p}{(2\pi)^{\frac{3}{2}}}\hat{A}_p(\vec{w}_p, z) & \left[ \hat{A}_s^\dagger(\vec{w}_p - \vec{w}_i - \vec{G}_x, z)e^{-i\mathcal{D}_1(\vec{w}_p - \vec{w}_i - \vec{G}_x, \vec{w}_p)z} + \right. \\ & \left. + \hat{A}_s^\dagger(\vec{w}_p - \vec{w}_i + \vec{G}_x, z)e^{-i\mathcal{D}_2(\vec{w}_p - \vec{w}_i + \vec{G}_x, \vec{w}_p)z} \right] \end{aligned} \quad (3)$$

$$\frac{\partial}{\partial z}\hat{A}_p(\vec{w}_p, z) = -\chi \int \frac{d^3\vec{w}_s}{(2\pi)^{\frac{3}{2}}}\hat{A}_s(\vec{w}_s, z) \left[ \hat{A}_i(\vec{w}_p - \vec{w}_s - \vec{G}_x, z)e^{i\mathcal{D}_1(\vec{w}_s, \vec{w}_p)z} + \hat{A}_i(\vec{w}_p - \vec{w}_s + \vec{G}_x, z)e^{i\mathcal{D}_2(\vec{w}_s, \vec{w}_p)z} \right] \quad (4)$$

where  $\vec{G}_x = (G_x, 0, 0)$  is a short-hand notation for the x-component of the reciprocal lattice vector in the 3D Fourier space, and  $\chi \simeq d_{01} \sqrt{\frac{\hbar\omega_s\omega_i\omega_p}{8\epsilon_0 c^3 n_i n_s n_p}}$ . The first and second term at r.h.s of these equations describe all the possible three-photon interactions  $\vec{w}_p \longleftrightarrow \vec{w}_s \vec{w}_i$  that satisfy the generalized energy-momentum conservation by means of the lattice vectors  $\vec{G}_1$  and  $\vec{G}_2$ , respectively :

$$\Omega_s + \Omega_i = \Omega_p \quad \text{energy conservation} \quad (5a)$$

$$\vec{q}_s + \vec{q}_i = \vec{q}_p \mp G_x \vec{e}_x \quad \text{transverse momentum conservation} \quad (5b)$$

$$k_{sz} + k_{iz} = k_{pz} - G_z \quad \text{longitudinal momentum conservation} \quad (5c)$$

The last rule, rigorously obeyed only for an infinite propagation length, is accounted for by the QPM functions:

$$\begin{aligned} \mathcal{D}_1(\vec{w}_s, \vec{w}_p) &= k_{sz}(\vec{w}_s) + k_{iz}(\vec{w}_p - \vec{w}_s - \vec{G}_x) - k_{pz}(\vec{w}_p) + G_z \\ \mathcal{D}_2(\vec{w}_s, \vec{w}_p) &= k_{sz}(\vec{w}_s) + k_{iz}(\vec{w}_p - \vec{w}_s + \vec{G}_x) - k_{pz}(\vec{w}_p) + G_z \end{aligned} \quad (6)$$

which contain the effects of temporal dispersion and diffraction at any order.

These equations are in general too complicated to be solved without approximations, but stochastic simulations can be performed in the medium-high gain regime of PDC in the framework of the Wigner representation, where the field operators are replaced by c-number fields [18]. In this context, the vacuum fluctuations at the crystal entrance facet are simulated by Gaussian white noise. The propagation equations are then integrated with a pseudo-spectral method, splitting linear propagation, solved in Fourier space, from nonlinear propagation solved in direct space. The linear part of the evolution is evaluated by using empirical Sellmeier formulas, found in [19] for the LiTaO<sub>3</sub> crystal. Quantum expectation values (in symmetric ordering) can be obtained by averaging over the initial conditions. A single stochastic realization can be taken as a semiclassical simulation of the system. Indeed, despite the unavoidable limitations of the size of the numerical grid (typically 512 x 256 x 512 points in the x, y and t directions), such simulations were able to closely reproduce, also quantitatively, the classical features of optical parametric generation in a HexNPC observed in [14].

## II. PARAMETRIC LIMIT AND SHARED MODES

Analytic results can be derived in the *parametric limit* where the pump beam, undepleted by the down-conversion process, is approximated as a classical plane-wave of constant amplitude along the sample. In this limit, by assuming that the input pump propagates in the  $(x, z)$  plane at an angle  $\theta_p \simeq \frac{q_p}{k_p} \ll 1$  with the  $z$ -axis, we can set  $\hat{A}_p(x, y, t, z) \rightarrow \alpha_p e^{iq_p x}$  where  $\alpha_p$  is the classical field amplitude. Linear evolution equations for the signal and idler operators are then obtained from Eqs.(2,3), by letting  $\hat{A}_p(\vec{w}_p, z) \rightarrow (2\pi)^{3/2} \alpha_p \delta(\vec{w}_p - \vec{w}_{0p})$ , where  $\vec{w}_{0p} = (q_p, 0, 0)$ . Let us focus on a signal mode  $\vec{w}_s$ , for which

$$\frac{\partial}{\partial z}\hat{A}_s(\vec{w}_s, z) = g_0 \left[ \hat{A}_i^\dagger(\vec{w}_{0p} - \vec{w}_s - \vec{G}_x, z)e^{-i\mathcal{D}_1(\vec{w}_s)z} + \hat{A}_i^\dagger(\vec{w}_{0p} - \vec{w}_s + \vec{G}_x, z)e^{-i\mathcal{D}_2(\vec{w}_s)z} \right] \quad (7)$$

where  $g_0 = \chi\alpha_p$  is taken real for definiteness, and

$$\mathcal{D}_{1,2}(\vec{w}_s) \equiv \mathcal{D}_{1,2}(\vec{w}_s, \vec{w}_p = \vec{w}_{0p}) = k_{sz}(q_{sx}, q_{sy}, \Omega_s) + k_{iz}(q_p - q_{sx} \mp G_x, -q_{sy}, -\Omega_s) - k_{pz}(q_p, 0, 0) + G_z \quad (8)$$

are the QPM functions in the parametric limit. This equation needs to be coupled to the evolution of the two idler modes

$$\frac{\partial}{\partial z} \hat{A}_i(\vec{w}_{0p} - \vec{w}_s - \vec{G}_x, z) = g_0 \left[ \hat{A}_s^\dagger(\vec{w}_s, z) e^{-iD_1(\vec{w}_s)z} + \hat{A}_s^\dagger(\vec{w}_s + 2\vec{G}_x, z) e^{-iD_2(\vec{w}_s + 2\vec{G}_x)z} \right] \quad (9)$$

$$\frac{\partial}{\partial z} \hat{A}_i(\vec{w}_{0p} - \vec{w}_s + \vec{G}_x, z) = g_0 \left[ \hat{A}_s^\dagger(\vec{w}_s - 2\vec{G}_x, z) e^{-iD_1(\vec{w}_s - 2\vec{G}_x)z} + \hat{A}_s^\dagger(\vec{w}_s, z) e^{-iD_2(\vec{w}_s)z} \right] \quad (10)$$

forming in principle an infinite chain of coupled equations. However, in most cases, only one of the two nonlinear processes is effective, because for a given signal mode either  $D_1(\vec{w}_s) = 0$  or  $D_2(\vec{w}_s) = 0$ . Then the usual pair of parametric equations coupling two signal-idler conjugate modes is obtained. Noticeably, there exist special points which are shared by both processes, satisfying

$$D_1(\vec{w}_s) = D_2(\vec{w}_s) = 0. \quad (11)$$

As it can be easily verified from Eq.(8), the first equality requires that  $q_{sx} = q_p$ , i.e. all the shared modes are characterized by the same x-component of the wave-vector as the pump. The y-component wave-vector then depends on the frequency  $q_{sy} = q_{sy}(\Omega_s)$ , as determined by QPM (the second equality in Eq. (11)). Each shared signal mode is then coupled to two idler modes at  $q_{ix} = \mp G_x$ ,  $q_{iy} = -q_{sy}$ ,  $\Omega_i = -\Omega_s$ .

The dual situation occurs for a shared idler mode at  $q_{ix} = q_p$ , coupled to two signal modes at  $q_{sx} = \mp G_x$ . Notice that unless the pump satisfies the *resonance* condition  $q_p = \pm G_x$ , the shared signal and shared idler configurations are strictly incompatible, and the evolution of each shared mode with its coupled modes forms a closed set of three parametric equations that will be examined in the next Sec.III. Conversely, when the pump is tilted at  $q_p = \pm G_x$ , two triplets of 3-modes, initially uncoupled, merge into a system of 4 coupled modes, whose equations will be studied in Sec. IV.

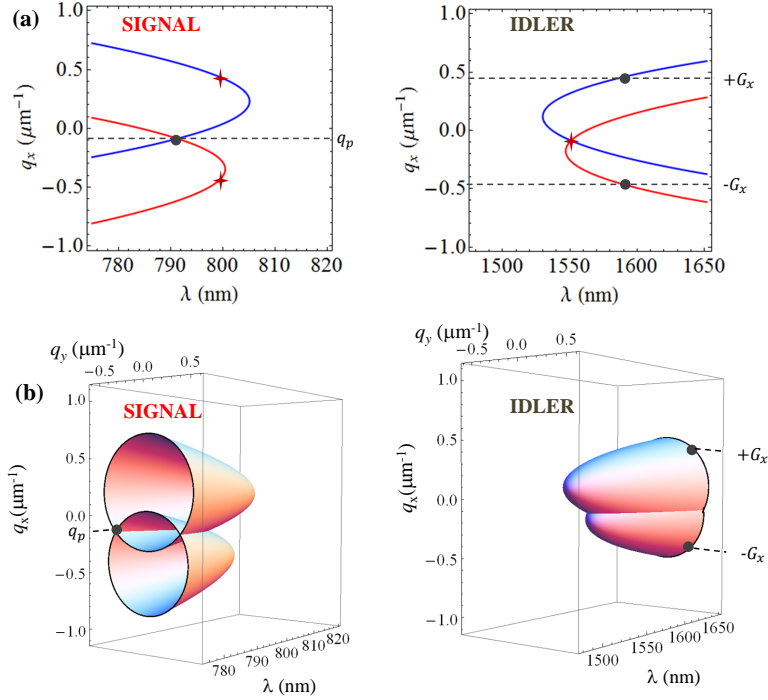


FIG. 2. QPM surfaces in the Fourier space (see text), calculated via the Sellmeier formulas in [19], for  $q_p = -0.3G_x$  (non resonant pump). For better readability  $\Omega$  has been mapped to the wavelength  $\lambda$ . (a) Projections along  $q_y = 0$  of the full 3D surfaces in (b). The bullets mark on-axis (a) and off-axis (b) examples of the 3 entangled modes, corresponding to a shared signal + 2 coupled idlers. The stars show the dual configuration with a shared idler+ two coupled signals. Parameters are those of the non-degenerate HexNPC crystal with  $\Lambda = 8.3\mu\text{m}$  used in [14].

Figs.2 and 3 show two examples of the QPM surfaces in the Fourier space, away from superresonance and at superresonance, respectively. In the signal panels, the lower and upper curves show the surfaces  $D_1(\vec{w}_s) = 0$  and  $D_2(\vec{w}_s) = 0$ , respectively, with the shared modes lying at their intersections. For the conjugate idler field, the same

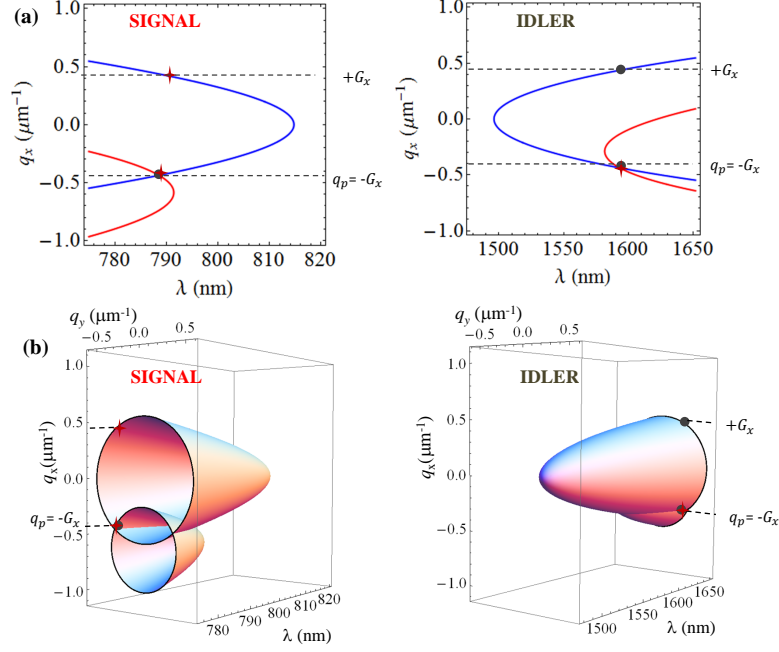


FIG. 3. Same as Fig.2 but at superresonance, with the pump tilted at  $q_p = -G_x$ . In this condition, all the shared modes superimpose to the lines of modes at  $q_x = -G_x$ , and two triplets of hot-spots merge into 4 coupled modes, as observed in [14].

surfaces are plotted as a function of  $\vec{w}_i = -\vec{w}_s + \vec{w}_{0p} \mp \vec{G}_x$ . The shared modes form continuous lines, which sit on the plane  $q_x = q_p$ ; their coupled modes also form continuous lines sitting on the two planes  $q_x = \mp G_x$ . When the pump is tilted at  $q_p = -G_x$ , all the shared modes superimpose to the lower coupled modes, and a sudden increase in the intensity at the location of these modes occur, as demonstrated in [14].

### III. 3-MODE ENTANGLEMENT

Let us focus on the shared signal configuration: we will show that away from superresonance this configuration realizes a 3-mode entangled state, which can be pictured as a parametric process of gain  $g = g_0\sqrt{2}$  followed by a beam splitter. The shared idler configuration can be treated in a completely analogous way.

Let us consider a signal mode  $\vec{w}_s = (q_p, q_{sy}, \Omega_s)$  shared by both processes, i.e. such that  $D_1(\vec{w}_s) = D_2(\vec{w}_s) := D(\vec{w}_s) \approx 0$ . It can be easily shown that sufficiently away from the condition  $q_p = \mp G_x$ , the modes  $\vec{w}_s \mp 2\vec{G}_x$  appearing in Eqs. (9) and (10) are not phase-matched, so that (II) reduce to a closed set of three equations, coupling the shared signal with the two idlers at  $q_x = \mp G_x$ . Let us give a short name to these modes

$$\hat{a}_{s0} := \hat{A}_s(q_p, q_{sy}, \Omega_s) \quad \text{shared signal at } q_p \quad (12)$$

$$\hat{a}_{i1} := \hat{A}_i(-G_x, -q_{sy}, -\Omega_s) \quad \text{coupled idler at } -G_x \quad (13)$$

$$\hat{a}_{i2} := \hat{A}_i(+G_x, -q_{sy}, -\Omega_s) \quad \text{coupled idler at } +G_x \quad (14)$$

Their evolution along the sample is described by

$$\frac{\partial}{\partial z} \hat{a}_{s0}(z) = g_0 \left[ \hat{a}_{i1}^\dagger(z) + \hat{a}_{i2}^\dagger(z) \right] e^{-iD(\vec{w}_s)z} \quad (15a)$$

$$\frac{\partial}{\partial z} \hat{a}_{i1}(z) = g_0 \hat{a}_{s0}^\dagger(z) e^{-iD(\vec{w}_s)z} \quad (15b)$$

$$\frac{\partial}{\partial z} \hat{a}_{i2}(z) = g_0 \hat{a}_{s0}^\dagger(z) e^{-iD(\vec{w}_s)z} \quad (15c)$$

These equations can be easily solved by introducing the canonical transformation  $\hat{a}_{i\pm} = \frac{\hat{a}_{i1} \pm \hat{a}_{i2}}{\sqrt{2}}$ , leading to:

$$\frac{\partial}{\partial z} \hat{a}_{s0}(z) = \sqrt{2}g_0 \hat{a}_{i+}^\dagger(z) e^{-i\mathcal{D}(\vec{w}_s)z} \quad (16a)$$

$$\frac{\partial}{\partial z} \hat{a}_{i+}(z) = \sqrt{2}g_0 \hat{a}_{s0}^\dagger(z) e^{-i\mathcal{D}(\vec{w}_s)z} \quad (16b)$$

$$\frac{\partial}{\partial z} \hat{a}_{i-}(z) = 0 \quad (16c)$$

The last equation simply means that the difference mode  $\hat{a}_{i-}$  is not affected by the parametric process: if at the crystal entrance face the idler field is in the vacuum state, then the difference between any two symmetrical idler modes at  $q_{ix} = \mp G_x$  remains in the vacuum. However, each of the two idler output modes has a nonzero intensity, because it has been parametrically amplified: as we shall see, this implies a correlation between the two idlers coupled via the same shared signal. The first two equations are the usual coupled equations, describing parametric generation for a pair of signal-idler conjugate modes, with an enhanced parametric gain

$$g = \sqrt{2}g_0 \quad (17)$$

As first shown in [10] and then demonstrated in [9, 11, 14], in the high-gain regime  $g_0 l_c \gg 1$ , this local gain enhancement gives rise to bright hot-spots in the parametric emission at the location of the three modes (see Fig.4 and 6). There,  $\langle \hat{a}_j^\dagger \hat{a}_j \rangle \propto \sinh^2(\sqrt{2}g_0 z) \simeq (e^{2g_0 z})^{\sqrt{2}}$ , ( $j = s0, i1, i2$ ), and the increase of intensity with respect to the background 2-mode fluorescence follows a power law  $I_{3\text{-mode}} = (I_{\text{background}})^{\sqrt{2}}$  [14]. Notice that in the direct space the sum and

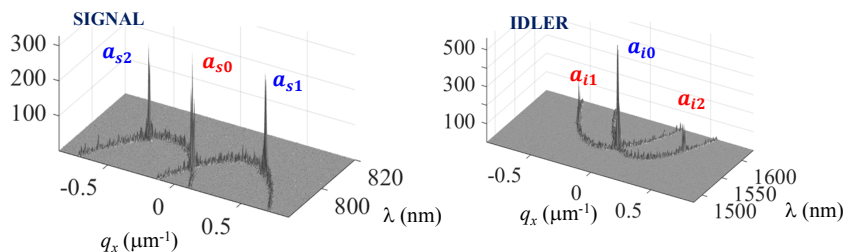


FIG. 4. Numerical simulations of the  $(\lambda, q_x)$  distributions of the signal and idler photon-numbers at the output of a HexNPC at  $q_y = 0$ , and for  $q_p = 0$  (non resonant pump). Two triplets of hot spots corresponding to the shared signal and shared idler configurations are evident. The pump is a 10ps Gaussian pulse centered at  $\lambda_p = 527.5\text{nm}$ , with a spatial Gaussian profile, of widths  $600\mu\text{m}$  and  $200\mu\text{m}$  in the x and y directions. The crystal length is  $l_c = 10\text{mm}$ , and  $g_0 l_c = 5$ .

difference modes have spatial modulations  $\sim \cos(G_x x)$ , and  $\sim \sin(G_x x)$ , respectively, in-phase and out-of-phase with the transverse modulation of the nonlinearity. Thus, the enhanced gain of the  $\hat{a}_{i+}$  mode can be interpreted as a spatial resonance with the nonlinear lattice.

Coming to the quantum properties of the state, the explicit solution of the two coupled parametric equations (16a) and (16b) can be found within the standard input-output formalism (see e.g. [20] for a summary), as a Bogoliubov transformation linking the quantum operators at the crystal exit face  $\hat{a}_j^{\text{out}} = \hat{a}_j(l_c)$  to those at the input  $\hat{a}_j^{\text{in}} = \hat{a}_j(0)$ , ( $j = s0, i+$ ):

$$\hat{a}_{s0}^{\text{out}} = U_\gamma(\vec{w}_s) \hat{a}_{s0}^{\text{in}} + V_\gamma(\vec{w}_s) \hat{a}_{i+}^{\text{in}} \quad (18a)$$

$$\hat{a}_{i+}^{\text{out}} = U_\gamma(\vec{w}_s) \hat{a}_{i+}^{\text{in}} + V_\gamma(\vec{w}_s) \hat{a}_{s0}^{\text{in}} \quad (18b)$$

Here  $\gamma = \sqrt{2} = g/g_0$  is a parameter giving the local gain enhancement in the hot-spots, and the explicit expressions of  $U_\gamma$  and  $V_\gamma$  can be found in Appendix A. A well known consequence of this transformation (see e.g. [21]) is that  $\hat{a}_{i+}$  is the twin beam of  $\hat{a}_{s0}$ , and their joint state is the *two-mode squeezed vacuum*. In the continuous-variable domain, the usual picture of twin-beam entanglement holds: the intensity fluctuations of  $\hat{a}_{i+}$  and  $\hat{a}_{s0}$  are perfectly correlated, and there is a "Einstein-Podolsky-Rosen" [22, 23] correlation between their field quadratures. Equations (18) have to be considered together with

$$\hat{a}_{i-}^{\text{out}} = \hat{a}_{i-}^{\text{in}} \quad (18c)$$

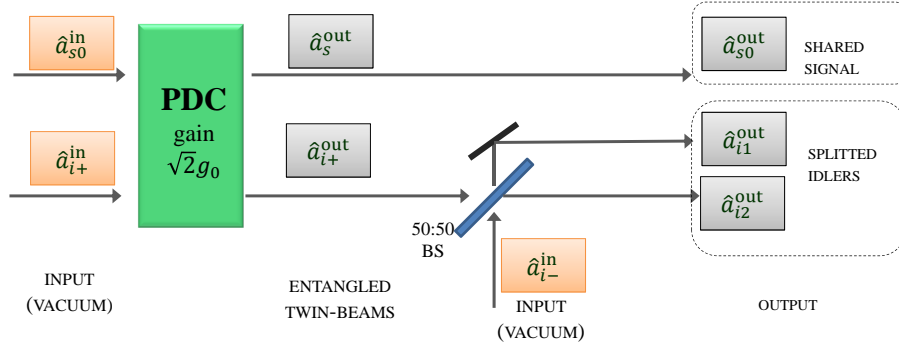


FIG. 5. Unfolding of the 3-mode entanglement generated by the HexNPC away from resonance, where a shared signal mode  $\hat{a}_{s0}$  is coupled to two idlers  $\hat{a}_{i1}$  and  $\hat{a}_{i2}$ . The process is equivalent to the a single PDC process generating maximally entangled twin beams, followed by the action of a 50:50 beam-splitter that mixes one of the entangled twins with an independent vacuum field (the difference between the two input idlers). As a result, tripartite entanglement is realized, with the two output idlers being entangled, but not perfectly, to the signal, and being correlated one to each other.

and the back-transformation

$$\hat{a}_{i1,2} = \frac{\hat{a}_{i+}^{out} \pm \hat{a}_{i-}^{out}}{\sqrt{2}}. \quad (18d)$$

Equations (18) are sufficient to calculate all the quantities of interest starting e.g. from a vacuum input. However, most of the properties of the 3-mode entanglement can be understood by noticing that the transformation (18d) can be formally described by the action of a 50:50 beam-splitter, mixing  $\hat{a}_{i+}^{out}$ , which is the twin beam of the shared signal  $\hat{a}_{s0}^{out}$ , with  $\hat{a}_{i-}^{out}$ , which trivially coincides with  $\hat{a}_{i-}^{in}$ . The overall process can be schematically pictured (Fig 5) as

- The action of a PDC device, generating the entangled twin beams  $\hat{a}_{s0}^{out}$ ,  $\hat{a}_{i+}^{out}$  with parametric gain  $g = \sqrt{2}g_0$ .
- Followed by a 50:50 beam-splitter acting on the idler arm, that mixes  $\hat{a}_{i+}^{out}$  with an independent mode  $\hat{a}_{i-}^{in}$ .

All of this is implemented by the nonlinear photonic crystal, which can be viewed as a sort of monolithic 3-mode nonlinear interferometer.

Clearly, each of the two splitted idlers is quantum entangled to the signal, even though the entanglement is not the maximal one of the twin beam, because of the random vacuum fluctuations of  $\hat{a}_{i-}^{in}$  entering the other port of the beam-splitter (assuming the difference mode is in a vacuum or coherent state). In addition, the coupling via the shared idler induces a certain degree of correlation between the splitted idler beams. Precisely :

- If the signal is *undetected*, the correlation between  $\hat{a}_{i1}^{out}$  and  $\hat{a}_{i2}^{out}$  is classical, and is equivalent to the correlation between the two outputs of a beam splitter illuminated by a thermal light beam. This follows straightforwardly from the well known fact that the marginal statistics of each twin beam, when considered independently from the other, is thermal-like. Then, in the high-gain the two idlers may possess a very high degree of mutual coherence, just as the splitted thermal beams used for thermal ghost imaging [24, 25], but their correlation is always shot-noise limited.
- If the signal is *detected*, the statistics of the coupled idlers, conditioned to detection (of some light observable) in the signal arm can be nonclassical, in particular they may show anticorrelated intensity fluctuations.

To clarify this last point, the problem can be reformulated in terms of the quantum state of the system. Let us focus on a specific shared-signal mode  $\vec{w}$ , with its coupled idlers (to be precise, one should also perform a discretization of Fourier modes, but it really does not matter). Given the input-output relations (18) for the transformed modes  $\hat{a}_{s0}$ ,  $\hat{a}_{i+}$ ,  $\hat{a}_{i-}$ , their output state can be written as:

$$|\psi'_{out}\rangle = \hat{R}_{s+}(\xi)\hat{1}_-|\psi_{in}\rangle \quad (19)$$

where the suffixes "s, +, -" refer to the shared signal, to the sum of the two idlers and to their difference, respectively,  $\hat{1}_-$  is the identity operator, and  $\hat{R}_{s+}(\xi) = \exp\left(\xi\hat{a}_{s0}^\dagger\hat{a}_{i+}^\dagger - \xi^*\hat{a}_{s0}\hat{a}_{i+}\right)$ , is the *two-mode squeeze operator*, acting on the

shared signal and the ” + ” mode. The squeeze parameter  $\xi$  can be related to the input-output coefficients in Eq.(18) (appendix A), and for phase-matched modes reduces to  $\xi = \sqrt{2}g_0l_c$ . Provided that the input state is vacuum, then

$$|\psi'_{out}\rangle = \left[ \sum_{N=0}^{\infty} c_N |N\rangle_s |N\rangle_+ \right] \otimes |0\rangle_- \quad (20)$$

where  $|N\rangle$  denotes the Fock state with N photons,  $|0\rangle$  is the vacuum state, and  $c_N = \frac{[U_\gamma(\bar{w})V_\gamma(\bar{w})]^N}{|U_\gamma(\bar{w})|^{2N+1}}$ , ( $\gamma = \sqrt{2}$ ). Incidentally, one can readily see that the reduced state in the idler arm is the thermal-like state:  $\hat{\rho}_\pm = \text{Tr}_s \{ |\psi'_{out}\rangle \langle \psi'_{out} \} = \left[ \sum_{N=0}^{\infty} |c_N|^2 |N\rangle_+ + |N\rangle_- \right] \otimes |0\rangle_- - \langle 0|$ .

For the original modes ( $\hat{a}_{s0}, \hat{a}_{i1}, \hat{a}_{i2}$ ), the state is then obtained as  $|\psi_{out}\rangle = \hat{B}_{+-} |\psi'_{out}\rangle$ , where  $\hat{B}_{+-}$  is the generator of the beam-splitter transformation  $\hat{B}_{+-} \hat{a}_\pm \hat{B}_{+-}^\dagger = \frac{\hat{a}_{i1} \pm \hat{a}_{i2}}{\sqrt{2}}$ . By using then standard properties of Fock states,

$$|\psi_{out}\rangle = \sum_{N=0}^{\infty} c_N |N\rangle_s \otimes \frac{1}{\sqrt{N!}} \left( \frac{\hat{a}_{i1}^\dagger + \hat{a}_{i2}^\dagger}{\sqrt{2}} \right)^N |0\rangle_1 |0\rangle_2 \quad (21)$$

$$= \sum_{N=0}^{\infty} c_N |N\rangle_s \left[ \sum_{k=0}^N \frac{1}{(\sqrt{2})^N} \sqrt{\frac{N!}{k!(N-k)!}} |k\rangle_1 |N-k\rangle_2 \right] \quad (22)$$

where the binomial expansion formula has been used to step to the second line. The result (22) is the sum of infinite terms: each of them is the product tensor of a state with N photons in the signal mode, times the superposition of all the possible partitions of the N twin idler photons into k photons in mode 1 and N-k photons in mode 2. Assuming that *exactly N photons* are detected in the signal arm the state of the two idler modes conditioned to this measurement is

$$|\psi_{idler}/N \text{ signal photon}\rangle = \frac{s \langle N | \psi_{out} \rangle}{\|s \langle N | \psi_{out} \rangle\|} = \sum_{k=0}^N \frac{1}{(\sqrt{2})^N} \sqrt{\frac{N!}{k!(N-k)!}} |k\rangle_1 |N-k\rangle_2 \quad (23)$$

This state is the N-photon path-entangled state, corresponding to the superposition of all the possible partitions of N photons into k photons in arm 1 and N-k photons in arm 2, with probability  $P_{k,N-k} = \frac{1}{2^N} \frac{N!}{k!(N-k)!}$  following the binomial distribution ( $\frac{1}{2}$  being the probability of taking either path for each photon). Such a state simply describes the random partition of the N photons in the two idler arms with equal probability of going one way or the other. It can be easily shown that the state is antibunched, and exhibits the maximum level of anticorrelation in the photon number fluctuations allowed by quantum mechanics. The simplest example is for  $N = 1$ ,

$$|\psi_{idler}/(1 \text{ signal photon})\rangle = \frac{1}{\sqrt{2}} (|0\rangle_1 |1\rangle_2 + |1\rangle_1 |0\rangle_2) \quad (24)$$

which is the path entangled single photon state explored in [5]. Conversely, when the signal is not detected, the state of the two splitted idlers is non-entangled because it is obtained by a linear transformation acting on the classical thermal state (but can be highly correlated and have mutual phase coherence [25, 26]).

We remind that in a full view of the problem, this 3-mode entangled state can be generated for a continuous range of Fourier modes  $w_s$  satisfying the shared signal condition (11), as well as for their shared idler counterparts. These modes span a broad band of frequencies, as the  $q_y$  coordinate is varied, or in practice, as the y-direction is scanned in the far-field (see [14] Supplementary Information).

#### IV. GOLDEN RATIO ENTANGLEMENT

In this section we focus on a particular pump propagation direction, corresponding to a transverse spatial resonance between the pump and the nonlinear lattice. We demonstrate in this condition the emergence of a peculiar 4-mode entangled state, dominated by the *Golden Ratio* of the segment.

By tilting the pump direction away from the symmetry  $z$ -axis, the position in the far-field plane of the shared modes move along  $q_x$  jointly with  $q_p$ , while the position of the coupled modes remain fixed at  $q_x = \pm G_x$ . Thus, when  $q_p = \mp G_x$ , in each signal/idler beam the shared modes arrive to superimpose to one line of unshared mode to which they were originally uncoupled (Fig. 3). As a result, the three hot-spot lines of the signal and the idler far-fields degenerate into two lines symmetrically positioned at  $q_x = \pm G_x$  (Fig.7), with a sudden increase of their intensity [14].



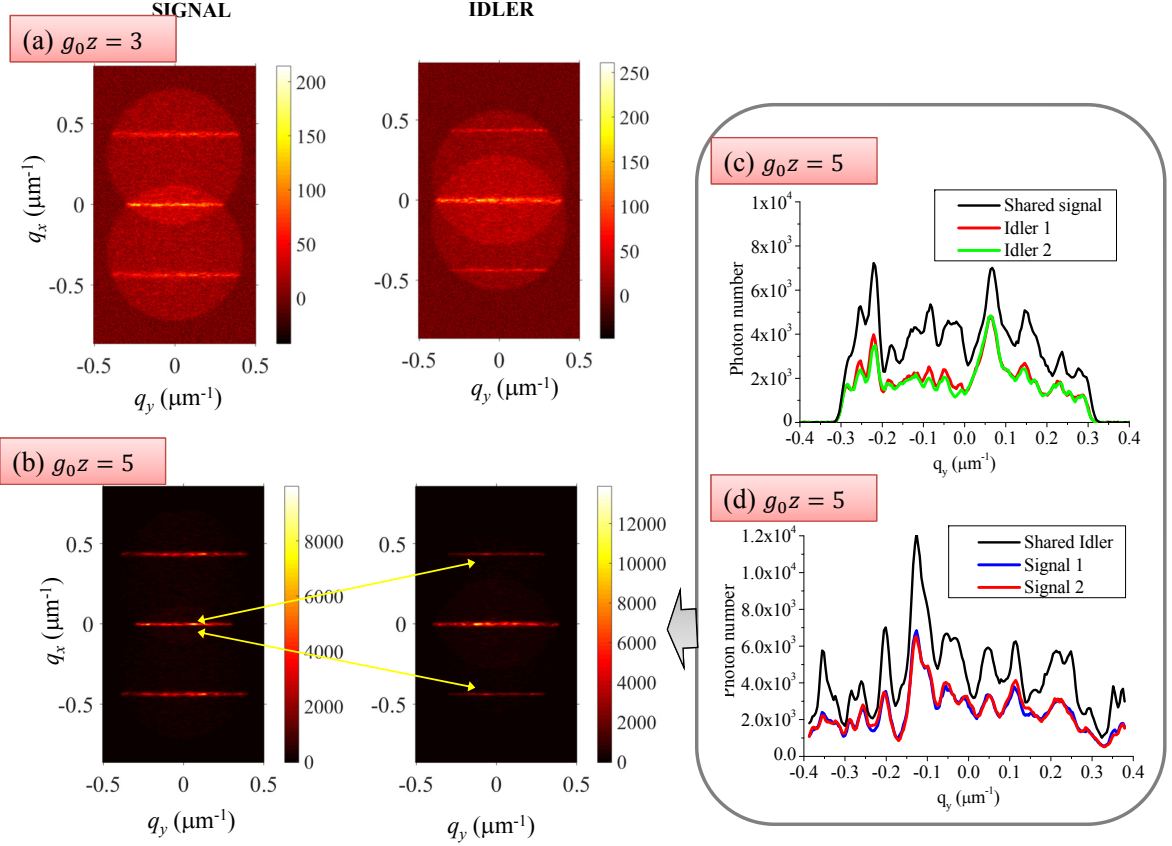


FIG. 6. (a) and (b) Numerical simulations of the  $(q_x, q_y)$  photon-number distributions (integrated over a single pump shot), for  $q_p = 0$ , showing the emergence of hot-spot lines for increasing propagation distance. Shared modes are located at  $q_x = q_p = 0$ , while their coupled modes are at  $q_x = \mp G_x$ . (c) Sections along  $q_y$ , highlighting a spatial correlation among the intensity fluctuations of the three modes ( $\hat{a}_{s0}, \hat{a}_{i1}, \hat{a}_{i2}$ ). Notice that the idler distributions have been mirrored  $q_y \rightarrow -q_y$ . (d) Same as (c) for the shared idler configuration. Other parameters as in Fig. 4.

We can describe this phenomenon as a *spatial resonance* between the pump and the lattice, because the pump has a transverse modulation (in its phase, not in its intensity) with the same spatial periodicity  $\Lambda_x = \frac{2\pi}{G_x}$  as the nonlinear grating. Notice that in this conditions the same modulation characterizes all the hot-spots of the down-converted beams.

Let us assume for definiteness  $q_p = -G_x$ , so that shared and coupled modes merge at  $q_x = -G_x$ . If we focus on a specific y-direction and on pair of conjugate signal idler frequencies (Fig.7), two triplets of hot spots which were originally uncoupled coalesce into 4 coupled modes. Let us give a name to these modes, as in the scheme of Fig. 8:

$$\hat{b}_s := \hat{A}_s(-G_x, q_{sy}, \Omega_s) \quad \hat{b}_i := \hat{A}_i(-G_x, -q_{sy}, -\Omega_s) \quad \text{shared modes at } -G_x \quad (25)$$

$$\hat{c}_s := \hat{A}_s(+G_x, q_{sy}, \Omega_s) \quad \hat{c}_i := \hat{A}_i(+G_x, -q_{sy}, -\Omega_s) \quad \text{unshared modes at } +G_x \quad (26)$$

Denoting by  $\vec{w}_s = (-G_x, q_{sy}, \Omega_s)$  the coordinate of the shared signal, the equations describing their evolution along

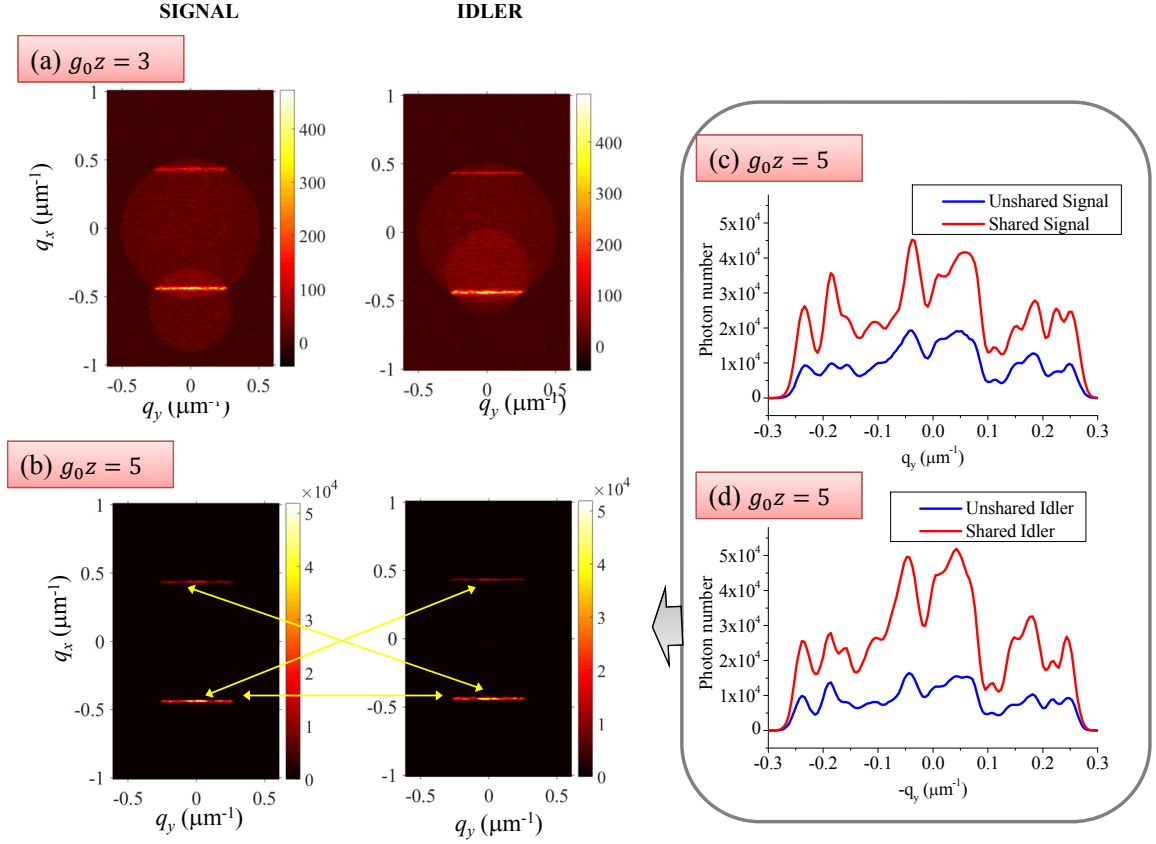


FIG. 7. Pump tilted at resonance  $q_p = -G_x$ . (a) and (b) Photon-number distributions in the  $(q_x, q_y)$  plane, at the output of a nondegenerate HexNPC, showing the emergence of 4 lines of hot-spots. Those at  $q_x = -G_x$  are shared by both processes (modes  $\hat{b}_s$  and  $\hat{b}_i$ ), while those at  $q_x = +G_x$  (modes  $\hat{c}_s$  and  $\hat{c}_i$ ) are unshared. The yellow arrows schematically show the coupling among the 4-modes. (c) Sections along  $q_y$  of the signal hot spots. (d) Same for the idler but mirrored  $q_y \rightarrow -q_y$ , in order to evidence the correlation. Other parameters as in Fig.4.

the sample take the closed form

$$\frac{\partial}{\partial z} \hat{b}_s(z) = g_0 [\hat{b}_i^\dagger(z) + \hat{c}_i^\dagger(z)] e^{-iD(\vec{w}_s)z} \quad (27a)$$

$$\frac{\partial}{\partial z} \hat{c}_s(z) = g_0 \hat{b}_i^\dagger(z) e^{-iD(\vec{w}_s)z} \quad (27b)$$

$$\frac{\partial}{\partial z} \hat{b}_i(z) = g_0 [\hat{b}_s^\dagger(z) + \hat{c}_s^\dagger(z)] e^{-iD(\vec{w}_s)z} \quad (27c)$$

$$\frac{\partial}{\partial z} \hat{c}_i(z) = g_0 \hat{b}_s^\dagger(z) e^{-iD(\vec{w}_s)z} \quad (27d)$$

It is not difficult to find their solutions in the spontaneous regime, that corresponds to the limit  $g_0 l_c \ll 1$ . As we shall see in the following, the mean number of photons in each of the 4 modes, at the leading order in  $g_0 z$  read

$$\langle \hat{b}_s^\dagger(z) \hat{b}_s(z) \rangle = \langle \hat{b}_i^\dagger(z) \hat{b}_i(z) \rangle = 2(g_0 z)^2 \text{sinc}^2 \left( \frac{D(\vec{w}_s)z}{2} \right) \delta(0) \quad (28)$$

$$\langle \hat{c}_s^\dagger(z) \hat{c}_s(z) \rangle = \langle \hat{c}_i^\dagger(z) \hat{c}_i(z) \rangle = (g_0 z)^2 \text{sinc}^2 \left( \frac{D(\vec{w}_s)z}{2} \right) \delta(0) \quad (29)$$

where the  $\delta(0)$  is an artificial divergence coming from the plane-wave pump approximation which can be easily

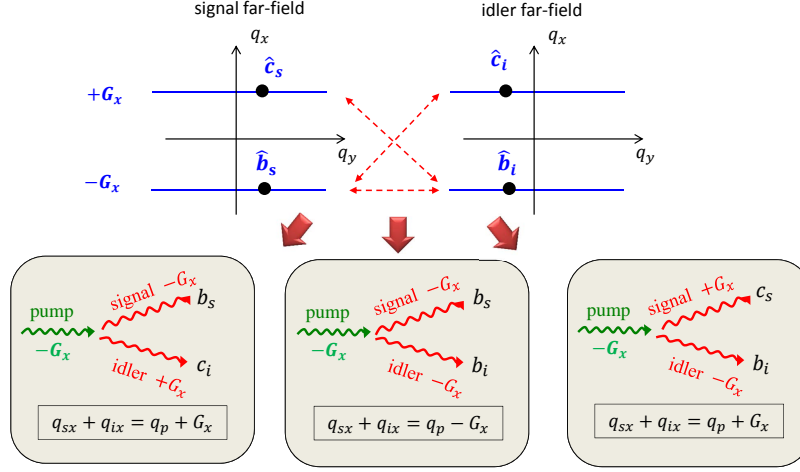


FIG. 8. Scheme of the coupling between the 4 modes at resonance, leading to Eqs.(27), and of the 3 microscopic down-conversion processes. The shared modes  $\hat{b}_j$  are populated by two processes out of the three. In the spontaneous regime, modes  $\hat{b}_j$  are twice as intense as the unshared modes  $\hat{c}_j$ , while in the stimulated regime the ratio between the two intensities is  $\phi^2$ .

removed<sup>1</sup>. Thus, we see that in the spontaneous regime modes  $\hat{b}_j$  are twice as populated as modes  $\hat{c}_j$ . This is natural because out of the three microscopic processes allowed by energy-momentum conservation, two of them contribute to the population of e.g the shared signal mode  $\hat{b}_s$ , and only one process contributes to the population of the unshared mode  $\hat{c}_s$ , as shown in Fig. 8b.

The situations changes in the stimulated regime of PDC. Indeed, the linear system (27) can be solved for any value of  $g_0$ , by introducing the transformation

$$\begin{pmatrix} \hat{\delta}_j \\ \hat{\sigma}_j \end{pmatrix} = \begin{pmatrix} \frac{1}{\sqrt{1+\phi^2}} & \frac{-\phi}{\sqrt{1+\phi^2}} \\ \frac{\phi}{\sqrt{1+\phi^2}} & \frac{1}{\sqrt{1+\phi^2}} \end{pmatrix} \begin{pmatrix} \hat{b}_j \\ \hat{c}_j \end{pmatrix} \quad (j = s, i) \quad (30)$$

where  $\phi$  is the so called *Golden Ratio* of the segment

$$\phi = \frac{1 + \sqrt{5}}{2} = 1.618.. \quad (31)$$

This sort of magic irrational number [27] is the solution to the problem of partitioning a segment into two parts  $b$  and  $c$ , whose ratio is equal to the ratio between the total length of the segment and the longer part:  $\frac{b}{c} = \frac{b+c}{b} = \phi$ . The Golden ratio can be also put in relation with the Fibonacci sequence (see e.g [28], [27]), and is the asymptotic value to which the ratio between two consecutive numbers in the sequence converge. With few steps which makes use of the properties of the Golden ratio, the original 4-mode equations can be decoupled into two independent systems

$$\begin{cases} \frac{\partial}{\partial z} \hat{\sigma}_s(z) = g_0 \phi \hat{\sigma}_i^\dagger(z) e^{-iD(\bar{w}_s)z} \\ \frac{\partial}{\partial z} \hat{\sigma}_i(z) = g_0 \phi \hat{\sigma}_s^\dagger(z) e^{-iD(\bar{w}_s)z} \end{cases} \quad (32)$$

and

$$\begin{cases} \frac{\partial}{\partial z} \hat{\delta}_s(z) = -\frac{g_0}{\phi} \hat{\delta}_i^\dagger(z) e^{-iD(\bar{w}_s)z} \\ \frac{\partial}{\partial z} \hat{\delta}_i(z) = -\frac{g_0}{\phi} \hat{\delta}_s^\dagger(z) e^{-iD(\bar{w}_s)z} \end{cases} \quad (33)$$

Notice that the transformation (30) is canonical, i.e. such that  $\hat{\sigma}_j$  and  $\hat{\delta}_j$  are independent photon annihilation operators, and that the two linear systems (32) and (33) are the standard equations describing parametric amplification

<sup>1</sup> the  $\delta(0)$  will then be replaced by a term  $\propto \frac{1}{\Delta\Omega_p \Delta q_p^2}$ , where  $\Delta\Omega_p, \Delta q_p$  are the temporal and spatial frequency bandwidths of the pump

in a pair of conjugate signal-idler modes. Thus, each of them generates a pair of independent twin beams, where modes  $\hat{\sigma}_s, \hat{\sigma}_i$  are characterized by an enhanced gain/squeeze parameter:

$$g_0 \rightarrow g_0 \times \phi = g_0 \times 1.618\dots, \quad (34)$$

whereas the gain/squeeze parameter is reduced for modes  $\hat{\delta}_s, \hat{\delta}_i$ :

$$g_0 \rightarrow -\frac{g_0}{\phi} = -g_0 \times 0.618\dots \quad (35)$$

Their explicit solutions can be written within the input-output formalism (Appendix A) as:

$$\hat{\sigma}_s^{out} = U_\phi(\vec{w}) \hat{\sigma}_s^{in} + V_\phi(\vec{w}) \hat{\sigma}_i^{\dagger in} \quad (36a)$$

$$\hat{\delta}_s^{out} = U_{-\frac{1}{\phi}}(\vec{w}) \hat{\delta}_s^{in} + V_{-\frac{1}{\phi}}(\vec{w}) \hat{\delta}_i^{\dagger in} \quad (36b)$$

and analog transformations for the output idlers, obtained by exchanging the indexes  $s \leftrightarrow i$ . These solutions have to be considered together with the inverse transformation

$$\begin{pmatrix} \hat{b}_j \\ \hat{c}_j \end{pmatrix} = \begin{pmatrix} \frac{1}{\sqrt{1+\phi^2}} & \frac{\phi}{\sqrt{1+\phi^2}} \\ \frac{-\phi}{\sqrt{1+\phi^2}} & \frac{1}{\sqrt{1+\phi^2}} \end{pmatrix} \begin{pmatrix} \hat{\delta}_j \\ \hat{\sigma}_j \end{pmatrix} \quad (j = s, i) \quad (36c)$$

We notice that the original modes  $\hat{b}_j, \hat{c}_j$  can be obtained from modes  $\hat{\sigma}_j$  and  $\hat{\delta}_j$  (and viceversa) via the action of a non balanced beam splitter with reflection and transmission coefficients  $t = \frac{1}{\sqrt{1+\phi^2}}$ ,  $r = \frac{\phi}{\sqrt{1+\phi^2}}$ , as  $\hat{b}_j = t\hat{\delta}_j + r\hat{\sigma}_j$ ,  $\hat{c}_j = -r\hat{\delta}_j + t\hat{\sigma}_j$ . Therefore, in the resonant case, the 4-mode entanglement can be considered equivalent to (see Fig. 9):

- Two independent parametric processes, with different gain parameters  $g_0\phi$  and  $-g_0/\phi$ , generating two independent pairs of entangled twin- beams in modes  $\sigma_j$  and  $\delta_j$ ;
- Followed by a non-balanced beam splitter that performs a "golden partition" of the two twins into the original modes

We thus see that a resonant pump provides the maximal coherence between the two nonlinear processes that coexist in the HexNPC . Indeed, away from this resonance, the 3-mode entanglement generated by the HexNPC is equivalent to a single nonlinear process (as depicted in Fig.5) generating bipartite entanglement, followed by a beam-splitter acting on one of the two parties. Conversely, when the pump resonates with the lattice, the output of the device is equivalent to *two* independent nonlinear processes generating two bipartite entangled states, followed by a linear device that mixes them.

This maximal coherence is also reflected into an enhancement of the intensity of hot-spots at resonance, experimentally observed in [14]. The mean photon numbers can be calculated from the solutions (36) as

$$\begin{aligned} \langle \hat{b}_j^{\dagger out} \hat{b}_j^{out} \rangle &= \frac{\phi^2}{1+\phi^2} \langle \hat{\sigma}_j^{\dagger out} \hat{\sigma}_j^{out} \rangle + \frac{1}{1+\phi^2} \langle \hat{\delta}_j^{\dagger out} \hat{\delta}_j^{out} \rangle \\ &= \delta(0) \left[ \frac{\phi^2}{1+\phi^2} |V_\phi(\vec{w}_s)|^2 + \frac{1}{1+\phi^2} |V_{-\frac{1}{\phi}}(\vec{w}_s)|^2 \right] \end{aligned} \quad (37)$$

$$\rightarrow \delta(0) \frac{\phi^2}{1+\phi^2} \sinh^2(g_0\phi l_c) \quad \text{for } g_0 l_c \gg 1 \quad (38)$$

$$\begin{aligned} \langle \hat{c}_j^{\dagger out} \hat{c}_j^{out} \rangle &= \frac{1}{1+\phi^2} \langle \hat{\sigma}_j^{\dagger out} \hat{\sigma}_j^{out} \rangle + \frac{\phi^2}{1+\phi^2} \langle \hat{\delta}_j^{\dagger out} \hat{\delta}_j^{out} \rangle \\ &= \delta(0) \left[ \frac{1}{1+\phi^2} |V_\phi(\vec{w}_s)|^2 + \frac{\phi^2}{1+\phi^2} |V_{-\frac{1}{\phi}}(\vec{w}_s)|^2 \right] \end{aligned} \quad (39)$$

$$\rightarrow \delta(0) \frac{1}{1+\phi^2} \sinh^2(g_0\phi l_c) \quad \text{for } g_0 l_c \gg 1 \quad (40)$$

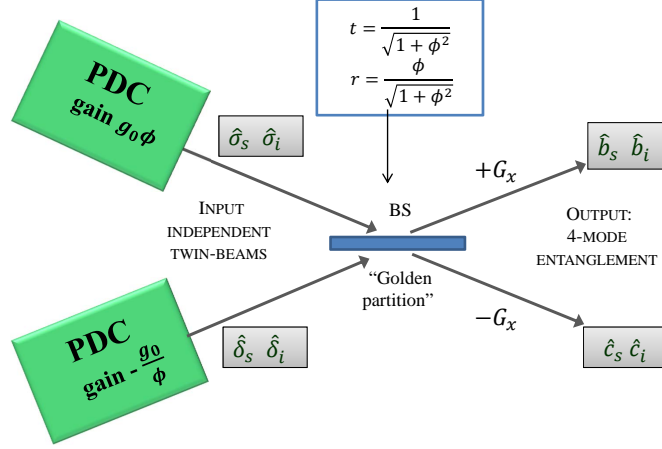


FIG. 9. Unfolding of the 4-mode entanglement generated in the hexagonal nonlinear photonic crystal at pump resonance. This can be considered equivalent to two independent parametric processes with gains  $g_0\phi$  and  $-g_0/\phi$ , mixed on a beam-splitter which makes a golden partition of the two pairs of twin beams into 4 entangled modes.

where the last lines hold for phase-matched modes  $D = 0$  and in the regime of stimulated PDC, i.e for  $g_0l_c \gg 1$ , where the mode intensities grow exponentially with  $g_0z$ . In such conditions, the contribution of modes  $\delta$  with smaller gain becomes negligible, and, as observed in [14] the local enhancement of intensity in the hot-spots is ruled by the Golden ratio:  $I_{4-modes} \simeq e^{2g_0\phi l_c} = (I_{\text{background}})^\phi$ . The Golden Ratio also rules the ratio between the amplitudes of the shared and unshared modes because  $\langle \hat{b}_j^{\dagger out} \hat{b}_j^{out} \rangle / \langle \hat{c}_j^{\dagger out} \hat{c}_j^{out} \rangle \rightarrow \phi^2$ .

Conversely, in the spontaneous PDC limit, by using the asymptotic behaviour of the functions  $V_\gamma$  provided in Appendix A, the expressions (37), (39) reduce to Eqs(29), where the Golden ratio does not appear and the ratio of the intensities of the shared and unshared mode is just 2. In this connection, it is also interesting to consider the quantum state generated by the HexNPC in the same limit This can be written in general as the state generated from the vacuum by the action of the two-mode squeeze operators acting on modes  $\sigma_j$  and  $\delta_j$  plus the action of the beam-splitter. As this is a rather cumbersome formula, we limit to its expression in the spontaneous regime ( $g_0l_c \ll 1$ ):

$$|\psi_{out}\rangle = \hat{B}_{\delta\sigma} \hat{R}_{\delta_s\delta_i}(\xi_{-1/\phi}) \hat{R}_{\sigma_s\sigma_i}(\xi_\phi) |\psi_{in}\rangle$$

$$\stackrel{g_0l_c \ll 1}{\simeq} |0\rangle + g_0l_c \text{sinc}\left(\frac{D(\vec{w}_s)l_c}{2}\right) e^{-i\frac{D(\vec{w})l_c}{2}} \left[ \hat{b}_s^\dagger \hat{c}_i^\dagger + \hat{b}_s^\dagger \hat{b}_i^\dagger + \hat{c}_s^\dagger \hat{b}_i^\dagger \right] |0\rangle \quad (41)$$

In this equation the contributions of the three microscopic processes allowed by energy-momentum conservation depicted in Fig.8 are evident. Since they take place with the same probability, in the spontaneous regime where the elementary down-conversion processes occur independently, the ratio of the two intensities is 2, and the Golden Ratio does not appear. This number appears only asymptotically, as the chain of stimulated processes become longer and longer.

One can recognize here an analogy with the Fibonacci sequence, defined by the recurrence relation  $F_{n+1} = F_n + F_{n-1}$ , with initial values  $F_1 = F_2 = 1$ . As well known [27], the ratio between two consecutive numbers  $\frac{F_{n+1}}{F_n}$  goes asymptotically to the Golden Ratio  $\phi$  for  $n \rightarrow \infty$ . Indeed, by considering the  $D = 0$  case, introducing proper hermitian quadrature operators, and the normalized distance  $\bar{z} = g_0z$ , the dynamical evolution of the amplitudes of modes  $b$  and  $c$  in Eqs. (27) can be reformulated as the simpler model <sup>2</sup>

$$\frac{dB}{d\bar{z}} = B + C$$

$$\frac{dC}{d\bar{z}} = B \quad (42)$$

whose eigenvalues  $\phi$  and  $-\frac{1}{\phi}$  are the solution of the quadratic characteristic equations  $\lambda^2 = \lambda + 1$ . It is possible to write a discrete version of the continuous evolution in Eq.(42), introducing  $B_n = B(n\Delta z), C_n = C(n\Delta z)$ , where

<sup>2</sup> Precisely, these equations describe the evolution of the most amplified field quadratures in the resonant case  $\hat{B} = \frac{1}{\sqrt{2}} (\hat{b}_s + \hat{b}_i + \hat{b}_s^\dagger + \hat{b}_i^\dagger)$ ,  $\hat{C} = \frac{1}{\sqrt{2}} (\hat{c}_s + \hat{c}_i + \hat{c}_s^\dagger + \hat{c}_i^\dagger)$ .

$\Delta z = z/n$  is a discrete step. It can be then demonstrated that at the  $n$ -th layer the amplitudes obey the Fibonacci-like recursive relations  $B_{n+1} = (2 + \Delta z)B_n + (\Delta z^2 - 1 - \Delta z)B_{n-1}$ . A similarity then holds with the famous description of the evolution of the population of rabbits introduced in the 13th century by L. Fibonacci [28]

$$\begin{aligned} F_{n+1} &= F_n + N_n \\ N_{n+1} &= F_n \end{aligned} \quad (43)$$

where  $F_n$  and  $N_n$  are the number of adult and newly born rabbits at month  $n$ , respectively. With initial conditions  $N_1 = 0, F_1 = 1$ , the solution is the Fibonacci sequence  $F_n = \frac{\phi^n - (-1/\phi)^n}{\sqrt{5}}$ . Clearly the analogy is limited, also because the quadratures in Eqs.(42) are not integer, since they are initiated by vacuum fluctuations, but the two models share the same eigenvalues (the Golden Ratio and its inverse), exhibiting an exponential and a geometrical growth rate, in the case of Eq.(42) and Eq.(43), respectively. Interestingly, the asymptotic behaviour of the ratio between the two variables is also preserved:  $\lim_{\bar{z} \rightarrow \infty} \frac{B(\bar{z})}{C(\bar{z})} = \lim_{n \rightarrow \infty} \frac{F_n}{N_n} = \phi$ .

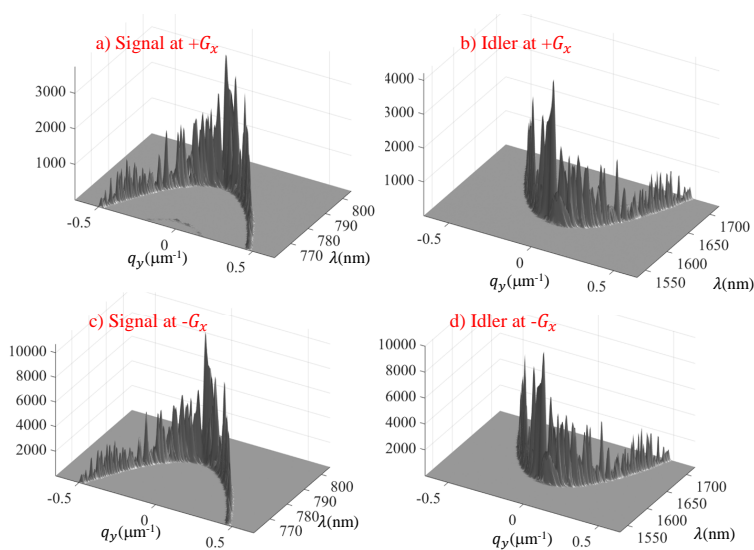


FIG. 10. Spectra of the hot-spots at superresonance ( $q_p = -G_x$ ) as the  $q_y$  coordinate is varied. Numerical simulations of the photon-number distributions in the  $(q_y, \lambda)$  plane at  $q_x = +G_x$  (a,b) and  $q_x = -G_x$  (b,c). Other parameters as in Fig.4.

As already remarked for the 3-mode case, also the Golden Ratio entanglement is widely tunable. Indeed the 4-mode entangled state is generated for a continuous range of shared signal modes  $\vec{w}_s$ , spanning a broad band of frequencies as the  $q_y$  coordinate is scanned along the hot-spot lines. This is evidenced by Fig. 10 which show numerical simulations of the spectra of the hot-spots as the  $q_y$  coordinate is varied.

## V. CONCLUSIONS

In this work, we studied the quantum state of twin photons and twin beams generated by parametric down-conversion in a hexagonally poled photonic crystal. The latter is characterized by the coexistence of two nonlinear processes, and represents an interesting monolithic source of path entangled photonic states. In particular we presented a novel point of view of the tripartite state that can be produced and we described the peculiar 4-mode entangled state generated by proper angular tuning of the input pump, in a regime we refer to as superresonance.

Away from superresonance, our description generalizes and partially confirms the analysis performed by other authors [5] in the low gain regime. Indeed our analysis of the 3 mode entanglement, not limited to the two-photon state, shows that it is necessary to perform a conditional measurement on the shared mode to produce quantum entanglement in the other two coupled modes. In the absence of such a conditional measurement, the state of the coupled modes is a non-entangled state, exhibiting the classical correlation/coherence properties of splitted thermal beams. Therefore in spite of the interesting compactness of the device, we can see in this case a somehow trivial analogy with the output state from a beam-splitter.

In contrast, we have shown that the angular degrees of freedom of the pump can be used for a further engineering of the output state. In particular at superresonance, the 4-mode state thereby generated is definitely non-trivial, as

the spatial resonance of the pump with the lattice establishes a strong coherence between the two nonlinear processes that coexist in the hexagonal photonic crystal. The output of the device can be seen as two bipartite entangled states followed by a linear device that performs a golden partition. The curious appearance of the golden ratio in this physical system can be explained by recognizing the existence of an analogy between the dynamical evolution of the mode amplitudes and Fibonacci sequence.

Finally, the original aspect of our theoretical model has allowed to highlight the spectral and spatial tunability of the HexNPC, as the entanglement described is generated over a large frequency bandwidth and over a continuous range of Fourier modes, rendering this compact monolithic device appealing for different integrated quantum optics and optical parametric generation experiments, that may require a versatility in the generation or detection schemes.

### Appendix A: Solutions of coupled propagation equations

Let us consider the generic 2-mode coupled parametric equations

$$\frac{\partial}{\partial z} \hat{a}_s(\vec{w}, z) = \gamma g_0 \hat{a}_i^\dagger(-w, z) e^{-iD(\vec{w})z} \quad (\text{A1})$$

$$\frac{\partial}{\partial z} \hat{a}_i(-\vec{w}, z) = \gamma g_0 \hat{a}_s^\dagger(w, z) e^{-iD(\vec{w})z} \quad (\text{A2})$$

where  $\gamma$  is a gain enhancement factor, arising from a coherent superposition of the two nonlinear processes characteristic of the hexagonal nonlinear pattern:  $\gamma = 1$  for the background fluorescence (no coherence between the two processes),  $\gamma = \sqrt{2}$  for the 3-mode coupling;  $\gamma = \phi$  or  $\gamma = -1/\phi$  for the 4-mode coupling at resonance. In terms of input field operators, their solution at the crystal exit face  $z = l_c$  can be written as

$$\hat{a}_s(\vec{w}, l_c) = U_\gamma(\vec{w}) \hat{a}_s(\vec{w}, 0) + V_\gamma(\vec{w}) \hat{a}_i^\dagger(-\vec{w}, 0) \quad (\text{A3})$$

$$\hat{a}_i(-\vec{w}, l_c) = U_\gamma(\vec{w}) \hat{a}_i(-\vec{w}, 0) + V_\gamma(\vec{w}) \hat{a}_s^\dagger(\vec{w}, 0) \quad (\text{A4})$$

Alternativa

$$\hat{a}_s(\vec{w}, z) = U_\gamma(\vec{w}, z) \hat{a}_s(\vec{w}, 0) + V_\gamma(\vec{w}, z) \hat{a}_i^\dagger(-\vec{w}, 0) \quad (\text{A5})$$

$$\hat{a}_i(-\vec{w}, z) = U_\gamma(\vec{w}, z) \hat{a}_i(-\vec{w}, 0) + V_\gamma(\vec{w}, z) \hat{a}_s^\dagger(\vec{w}, 0) \quad (\text{A6})$$

where

$$U_\gamma(\vec{w}) = \left[ \cosh[\Gamma(\vec{w})l_c] + \frac{iD(\vec{w})}{2\Gamma(\vec{w})} \sinh[\Gamma(\vec{w})l_c] \right] e^{-i\frac{D(\vec{w})l_c}{2}}$$

$$V_\gamma(\vec{w}) = \gamma g_0 \frac{\sinh[\Gamma(\vec{w})l_c]}{\Gamma(\vec{w})} e^{-i\frac{D(\vec{w})l_c}{2}} \quad (\text{A7})$$

$$\Gamma(\vec{w}) = \sqrt{|\gamma g_0|^2 - \frac{D^2(\vec{w})}{4}}$$

In the low-gain limit where  $\gamma g_0 l_c \rightarrow 0$ , with  $Dl_c$  finite (spontaneous PDC limit), the coefficients take the familiar form  $U_\gamma(\vec{w}) \rightarrow 1$  and  $V_\gamma(\vec{w}) \rightarrow \gamma g_0 l_c \text{sinc}\left[\frac{D(\vec{w})l_c}{2}\right] e^{-i\frac{D(\vec{w})l_c}{2}}$ .

If instead of evolving the field along the sample, one chooses to work in the picture where the state evolves, then the output state is given by the action of the two-mode squeeze operator on the input state:

$$|\psi_{out}\rangle = \hat{R}(\xi) |\psi_{in}\rangle$$

$$\hat{R}(\xi) = e^{\xi(\vec{w}) \hat{a}_s^\dagger(\vec{w}) \hat{a}_i^\dagger(-w) - \xi(\vec{w})^* \hat{a}_s(\vec{w}) \hat{a}_i(-w)} \quad (\text{A8})$$

where the squeeze parameter  $\xi = r e^{2i\theta}$  is determined by the input-output coefficients as  $\tanh(r) = \frac{|V_\gamma|}{|U_\gamma|}$ ,  $\theta = \frac{1}{2} \arg[U_\gamma V_\gamma]$ . Notice that for phase matched modes for which  $D(w) = 0$ , it simply reduces to  $\xi = \gamma g_0 l_c$ .

---

[1] V. Berger, Phys. Rev. Lett. **81**, 4136 (1998).

- [2] A. Arie, N. Habshoosh, and A. Bahabad, *Optical and Quantum Electronics* **39**, 361 (2007).
- [3] A. Arie, A. Bahabad, and N. Habshoosh, “Nonlinear interactions in periodic and quasi-periodic nonlinear photonic crystals,” in *Ferroelectric Crystals for Photonic Applications: Including Nanoscale Fabrication and Characterization Techniques*, edited by P. Ferraro, S. Grilli, and P. De Natale (Springer Berlin Heidelberg, Berlin, Heidelberg, 2009) pp. 259–284.
- [4] Y.-X. Gong, P. Xu, Y. F. Bai, J. Yang, H. Y. Leng, Z. D. Xie, and S. N. Zhu, *Phys. Rev. A* **86**, 023835 (2012).
- [5] H. Jin, P. Xu, X. W. Luo, H. Y. Leng, Y. X. Gong, W. J. Yu, M. L. Zhong, G. Zhao, and S. N. Zhu, *Phys. Rev. Lett.* **111**, 023603 (2013).
- [6] E. Megidish, A. Halevy, H. S. Eisenberg, A. Ganany-Padowicz, N. Habshoosh, and A. Arie, *Opt. Express* **21**, 6689 (2013).
- [7] Y.-X. Gong, S. Zhang, P. Xu, and S. N. Zhu, *Opt. Express* **24**, 6402 (2016).
- [8] K. Gallo, M. Levenius, F. Laurell, and V. Pasiskevicius, *Appl. Phys. Lett.* **98**, 161113 (2011).
- [9] M. Levenius, V. Pasiskevicius, and K. Gallo, *Appl. Phys. Lett.* **101**, 121114 (2012).
- [10] H.-C. Liu and A. H. Kung, *Opt. Express* **16**, 9714 (2008).
- [11] L. Chen, P. Xu, Y. F. Bai, X. W. Luo, M. L. Zhong, M. Dai, M. H. Lu, and S. N. Zhu, *Opt. Express* **22**, 13164 (2014).
- [12] M. Conforti, F. Baronio, M. Levenius, and K. Gallo, *Opt. Lett.* **39**, 3457 (2014).
- [13] K. Stensson, G. Björk, and K. Gallo, in *Advanced Solid State Lasers* (Optical Society of America, 2014) p. ATu3A.5.
- [14] O. Jedrkiewicz, A. Gatti, E. Brambilla, M. Levenius, G. Tamošauskas, and K. Gallo, *Scientific Reports* **8** (2018), 10.1038/s41598-018-30014-7.
- [15] M. Levenius, *Optical Parametric Devices in Periodically Poled LiTaO<sub>3</sub>*, Ph.D. thesis, KTH, Quantum Electronics and Quantum Optics, QEO (2013).
- [16] A. Gatti, R. Zambrini, M. San Miguel, and L. A. Lugiato, *Phys. Rev. A* **68**, 053807 (2003).
- [17] E. Brambilla, O. Jedrkiewicz, P. D. Trapani, and A. Gatti, *J. Opt. Soc. Am. B* **31**, 1383 (2014).
- [18] A. Gatti, H. Wiedemann, L. A. Lugiato, I. Marzoli, G.-L. Oppo, and S. M. Barnett, *Phys. Rev. A* **56**, 877 (1997).
- [19] H. H. Lim, S. Kurimura, T. Katagai, and I. Shoji, *Jpn. J. Appl. Phys* **52**, 032601 (2013).
- [20] A. Gatti and E. Brambilla, *Int. J. of Quantum Inf.* **15**, 1740017 (2017).
- [21] C. C. Gerry and P. L. Knight, *Introductory Quantum Optics* (Cambridge University Press, 2005) Chap. 7, pp. 167–169,182–187.
- [22] A. Einstein, B. Podolsky, and N. Rosen, *Phys. Rev.* **47**, 777 (1935).
- [23] M. D. Reid, *Phys. Rev. A* **40**, 913 (1989).
- [24] A. Gatti, E. Brambilla, M. Bache, and L. A. Lugiato, *Phys. Rev. Lett.* **93**, 093602 (2004).
- [25] A. Gatti, M. Bache, D. Magatti, E. Brambilla, F. Ferri, and L. A. Lugiato, *J. of Modern Opt.* **53**, 739 (2006).
- [26] A. Gatti, E. Brambilla, M. Bache, and L. A. Lugiato, *Phys. Rev. A* **70**, 013802 (2004).
- [27] R. Dunlap, *The Golden Ratio and Fibonacci Numbers* (World scientific, 2017).
- [28] T. Koshy, *Fibonacci and Lucas Numbers with Applications* (John Wiley & Sons, 2011) Chap. 2.